Front. Phys., 2012, 7(4): 380–385
DOI 10.1007/s11467-012-0266-8

PERSPECTIVE

Multiferroic tunnel junctions

Yue-Wei Yin[1,2], **Muralikrishna Raju**[1], **Wei-Jin Hu**[1,3], **Xiao-Jun Weng**[4], **Ke Zou**[1], **Jun Zhu**[1], **Xiao-Guang Li**[2], **Zhi-Dong Zhang**[3], **Qi Li**[1,†]

[1] *Department of Physics, Pennsylvania State University, University Park, PA 16802, USA*

[2] *Hefei National Laboratory for Physical Sciences at Microscale, Department of Physics, University of Science and Technology of China, Hefei 230026, China*

[3] *Shenyang National Laboratory for Materials Science, Institute of Metal Research, Chinese Academy of Sciences, Shenyang 110016, China*

[4] *Department of Materials Science and Engineering, Materials Research Institute, Pennsylvania State University, University Park, PA 16802, USA*

E-mail: † *qil1@psu.edu*

Received July 10, 2012; accepted July 24, 2012

Magnetic tunnel junctions with ferroelectric barriers, often referred to as multiferroic tunnel junctions, have been proposed recently to display new functionalities and new device concepts. One of the notable predictions is that the combination of two charge polarizing states and the parallel and antiparallel magnetic states could make it a four resistance state device. We have recently studied the ferroelectric tunneling using a scanning probe technique and multiferroic tunnel junctions using ferromagnetic $La_{0.7}Ca_{0.3}MnO_3$ and $La_{0.7}Sr_{0.3}MnO_3$ as the electrodes and ferroelectric (Ba, Sr)TiO_3 as the barrier in trilayer planner junctions. We show that very thin (Ba, Sr)TiO_3 films can sustain ferroelectricity up till room temperature. The multiferroic tunnel junctions show four resistance states as predicted and can operate at room temperatures.

Keywords multiferroic tunnel junction, ferroelectric film, tunneling magnetoresistance effect, tunneling electroresisitance effect, magnetoelectric coupling

PACS numbers 75.85.+t, 77.55.fe, 75.70.Cn, 75.60.Ej, 77.80.Fm

1 Introduction

The demands for faster, smaller, and non-volatile electronics have pushed the limit of semiconductor devices to ever smaller dimensions. However, the challenge of power dissipation places a limit on the future device scaling. In addition, size effects may also post constraint on device miniaturization. These have led to an emergent need and development of new concepts for information processing and storage [1, 2]. For the next generation devices, multifunctional structures have been envisioned, which can perform new functionality, can be manipulated by several external independent controls, and can operate with low power [3, 4]. One of the approaches to multi-functional devices is to combine ferromagnetic (FM) based spintronics with ferroelectric (FE) based functionality [3, 4]. It can be used as memory cells with multiple resistance states or to combine logic and memory operations. It may also be able to achieve cross control of the spin and charge degrees of freedom. This offers significant opportunities for new device concepts.

Magnetic tunnel junctions (MTJs) is the most widely used spintronic device in computer read heads, sensors, and memories [5]. The parallel and antiparallel magnetization alignments of the two electrodes represent two logic states with different resistances (tunneling magnetoresistance, TMR). Ferroelectric tunneling refers to a tunnel junction using a ferroelectric as the barrier. The basic idea of an FTJ was raised by Esaki *et al.* [6] decades ago. However, it only aroused considerable research interest recently, largely because only in recent years experiments [7–9] have shown that ferroelectricity can persist down to the nanometer scale. This makes it possible to use ferroelectrics as tunneling barriers. The key property of an FTJ is the switching of junction resistance with the reversal of ferroelectric polarization, namely, tunneling electroresistance (TER) effect. As reviewed by Tsymbal

© Higher Education Press and Springer-Verlag Berlin Heidelberg 2012

et al. [10], the TER effect of an FTJ could at least be obtained through the following three effects: i) electrostatic effect which will change the depolarization potential through the asymmetrical screening of the two interfaces of the barrier [11]; ii) asymmetrical interface atomic arrangement that will influence the transmission probability by the ferroelectric ionic displacement at interfaces [12]; and iii) strain effect which will affect the barrier width due to the piezoelectricity effect [13]. Very recently large TER effect tested using a scanning probe technique has been reported on $BaTiO_3$ [14–16] and $PbZr_xTi_{1-x}O_3$ [17, 18] ferroelectric films.

Combining a magnetic tunnel junction with a ferroelectric barrier, i.e., a multiferroic tunnel junctions (MFTJs), will add new functionality beyond the single MTJs or FTJs. The junction resistance will be sensitive to not only the magnetization alignment of the electrodes, but also the polarization direction of the barrier. This makes MFTJ a quaternary-state device which can be switched by both electric and magnetic fields. Theoretical calculations on $SrRuO_3/BaTiO_3/SrRuO_3$ structure have predicted [19] about $\sim 50\%$ resistance differences between the two polarization states, making the MFTJ a practically useful device. Moreover, due to the mechanical coupling [20], chemical bonding [21] or spin dependent screening [22] at the ferromagnetic/ferroelectric interfaces, these artificial composites of ferroic materials may enable the magnetoelectric coupling effect (as reviewed by [3, 4, 23–26]), making it possible to control magnetization by electric field or control electric polarization by magnetic field.

The first reported MFTJ is another type of MFTJ employing a single phase multiferroic $La_{0.1}Bi_{0.9}MnO_3$ barrier in a $Au/La_{2/3}Sr_{1/3}MnO_3$ junction where the TMR is due to the spin filtering effect and the TER is related to the barrier potential change when polarization is reversed [27]. Recently, by using a Fe indentation technique, Garcia *et al.* have fabricated the nanoscale Fe (or Co)/$BaTiO_3/La_{0.7}Sr_{0.3}MnO_3$ ferroelectric/ferromagnetic/ferroelectric MFTJs and reported the control of carrier spin polarization by electrically reversing the ferroelectric polarization [28, 29]. Moreover, not only the magnitude, but also the signs of the TMR can be inverted by ferroelectric switching in $Co/PbZr_{0.2}Ti_{0.8}O_3/La_{0.7}Sr_{0.3}MnO_3$ MFTJs, showing a new method of spin control in spintronic devices [30]. The four resistance states have also been reported on all perovskite $La_{0.7}Sr_{0.3}MnO_3/BiFeO_3/La_{0.7}Sr_{0.3}MnO_3$ MFTJs where $BiFeO_3$ is an intrinsic multiferroic material [31]. However, all of these results showed small magnetoresistance and can work only at low temperatures.

To obtain both TMR and TER effects in a MFTJ, thin insulating barrier with persistent ferroelectricity and ferromagnetic electrodes with high spin polarization are critical. Here, we choose (Ba, Sr)TiO_3 as ferroelectric barrier which shows ferroelectricity down to one unit cell under proper strain condition [7] and half metallic $La_{0.7}Ca_{0.3}MnO_3$ (LCMO) and $La_{0.7}Sr_{0.3}MnO_3$ (LSMO) as ferromagnetic electrodes for the proper lattice match with the barrier [32]. Large TMR and TER effects have been observed in the LCMO-based MFTJs [33], and in LSMO-based MFTJs the four resistance states can be achieved even up to room temperature [34].

2 Experiment

Epitaxial (Ba, Sr)$TiO_3/La_{0.7}Sr_{0.3}MnO_3$ bilayers for piezoresponse force microscopy (PFM) measurements and $La_{0.7}Ca_{0.3}MnO_3$/(Ba, Sr)$TiO_3/La_{0.7}Ca_{0.3}MnO_3$and $La_{0.7}Sr_{0.3}MnO_3$/(Ba, Sr)$TiO_3/La_{0.7}Sr_{0.3}MnO_3$ trilayers for MFTJ investigations were grown on $SrTiO_3$ (100) substrates by pulsed laser deposition. The heterostructures were deposited *in situ* at 750°C in a 300 mTorr flowing oxygen. The laser energy density was about 1.5 J/cm^2. The epitaxial growth of the trilayers on $SrTiO_3$ is revealed by high-resolution transmission electron microscopy (TEM) and the TEM specimens were prepared using conventional mechanical polishing followed by Ar ion milling. Cross-sectional scanning TEM (STEM) was performed in a JEOL-2010F field-emission TEM/STEM operated at 200 keV. The ferroelectric property of the (Ba, Sr) TiO_3 ultrathin films were investigated by PFM [Asylum Research-MFP-3D atomic probe microscopy (AFM)].

The micron-scale MFTJ in the cross-strip geometry was fabricated by using photolithography and Ar ion milling in a process similar to what we have used before [35]. Sputtered MgO or SiO_2 was used as an insulating layer to allow making gold contact leads with the top electrode without shorting to the bottom electrode. The schematic drawing of the MFTJ structure is illustrated in Fig. 1(a). A four-probe method was used to do electrical transport measurement. The positive bias corresponds to the current flow from top to bottom electrode and the magnetic field was applied along the longitudinal direction of the bottom $La_{0.7}Sr_{0.3}MnO_3$ lead.

3 Results and discussion

To characterize the structural quality, X-ray diffraction θ–2θ and φ scans as well as high resolution cross sectional STEM have been conducted on selected samples. X-ray diffraction shows that all layers are grown epitaxially. Figure 1(b) is a high-resolution cross-sectional high-angle annular-dark-field (HAADF) STEM image of an as-grown $La_{0.7}Ca_{0.3}MnO_3/Ba_{0.5}Sr_{0.5}TiO_3/La_{0.7}Ca_{0.3}MnO_3$ trilayer. Almost atomically smooth growth of the $Ba_{0.5}Sr_{0.5}TiO_3$ barrier was obtained even for our relatively thick $La_{0.7}Ca_{0.3}MnO_3$ bottom

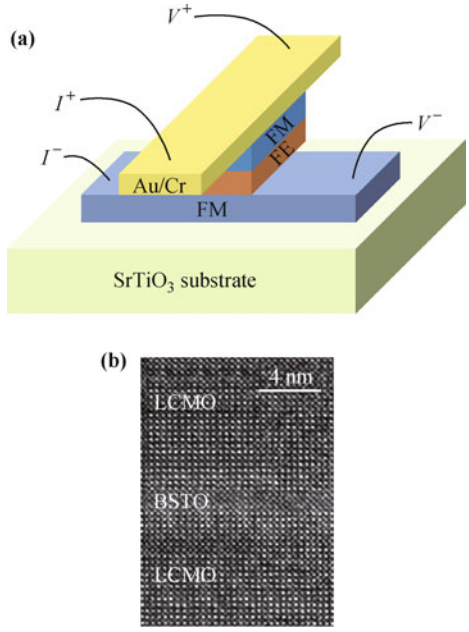

Fig. 1 **(a)** The schematic diagram of the MFTJ (the MgO or SiO_2 insulating layer between the top and bottom lead is not shown). **(b)** Cross-sectional HAADF STEM image of a $La_{0.7}Ca_{0.3}MnO_3$(LCMO)/$Ba_{0.5}Sr_{0.5}TiO_3$(BSTO)/$La_{0.7}Ca_{0.3}MnO_3$ trilayer.

film (∼30 nm), indicating high quality heterostructure growth.

To confirm the ferroelectricity of nanoscale (Ba, Sr)TiO_3 film, PFM and conducting atomic force microscopy (CAFM) have been performed at room temperature on several (Ba, Sr)TiO_3/$La_{0.7}Sr_{0.3}MnO_3$ samples. As illustrated in Fig. 2(a), these investigations were carried out based on a scanning probe microscopy (Asylum Research-MFP-3D AFM) using a conductive AFM tip in contact with the (Ba, Sr)TiO_3 surface. Figure 2(b) shows an out-of-plane PFM phase image at room temperature for a 3.5 nm $Ba_{0.95}Sr_{0.05}TiO_3$ thin film on top of a 30 nm $La_{0.7}Sr_{0.3}MnO_3$ bottom electrode. Here, a word "PSU" and the background were written by negative (−6.0 V) and positive (+6.0 V) voltages respectively. The observed "PSU" pattern indicates the occurrence of ferroelectric switching. Figure 1(b) shows a local voltage dependence of piezoresponse phase which suggests a ∼ 180° phase contrast and provides evidence for ferroelectricity of nanoscale (Ba, Sr)TiO_3 film. The current (I)–voltage (V) characteristic of this sample have also been tested by CAFM, as shown in Fig. 3. After polarize the ferroelectricity upward and downward, two obvious different I–V was observed. At −1 V, a large TER ∼30 000% was obtained.

In trilayer junction structures, due to the large junction area (∼ 10 μm × 10 μm) in comparison with the scanning probe contact area (with a diameter of about several tens of nanometers), large TER has not been reported presumably due to the weak links and multidomain structures when the ferroelectric barrier is poled to reverse its directions using a large voltage. In addition, it was proposed that the large TER observed from the PFM measurement without the top electrode is due to the surface absorption of elements which acted as an additional dielectric layer on top of the ferroelectric layer [36]. By increasing the asymmetry of the junction, the dielectric layer will serve as a switch changing its barrier height dramatically when the electrostatic potential is changed by polarization reversal, leading to the giant TER values in PFM test.

Figure 4(a) shows the non-linear I–V characteristic of a $La_{0.7}Sr_{0.3}MnO_3$/$Ba_{0.95}Sr_{0.05}TiO_3$/$La_{0.7}Sr_{0.3}MnO_3$ MFTJ (∼ 10 μm × 20 μm in area) at room temperature. The corresponding differential conductance $G = \mathrm{d}I/\mathrm{d}V$ shows a parabolic dependence on bias voltage, as can be seen in the normalized conductance $G(\mathrm{V})/G(0)$ shown in the inset of Fig. 4(a). As indicated by the solid line in the inset of Fig. 4(a), the good fitting of the conductance curve with Brinkman model [37] indicates that the electron tunneling dominates the transport process. Figure 4(b) shows potential diagrams drew based on the fitting parameters, the barrier thickness (d), average barrier height ($\bar{\varphi}$) and the asymmetry in the barrier ($\Delta\varphi$) for the curves with the barrier polarized downward and upward (with a poling voltage of $V_{\mathrm{pulse}} \approx +1.4$ V or −1.4 V). The differences between the barrier parameters after poling the ferroelectricity down or up suggest that the ferroelectricity can affect the electron transport properties of MFTJ, which will result in the TER effect. Similar to the theoretical prediction [19], the TER effect may be caused by the asymmetric $Ba_{0.95}Sr_{0.05}TiO_3$/$La_{0.7}Sr_{0.3}MnO_3$ interface which will induce asymmetric ferroelectric displacements in the barrier and lead to a change in

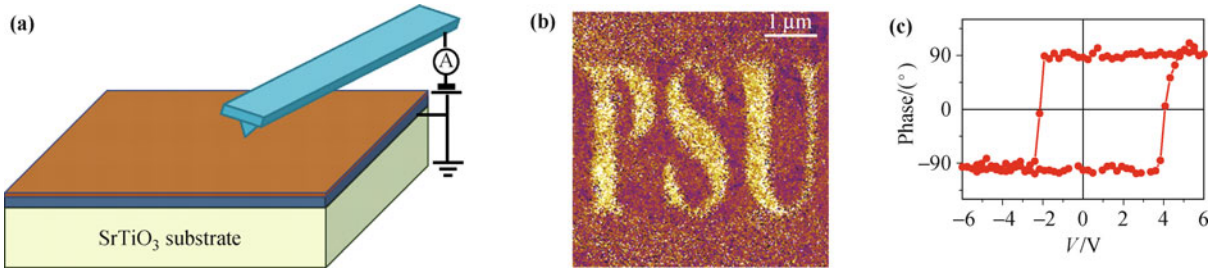

Fig. 2 **(a)** A shematic drawing of PFM and CAFM measurement setup. **(b)** Out of plane PFM phase image and **(c)** local PFM phase as a function of bias voltage of a 3.5 nm $Ba_{0.95}Sr_{0.05}TiO_3$ film on 30 nm $La_{0.7}Sr_{0.3}MnO_3$ electrode.

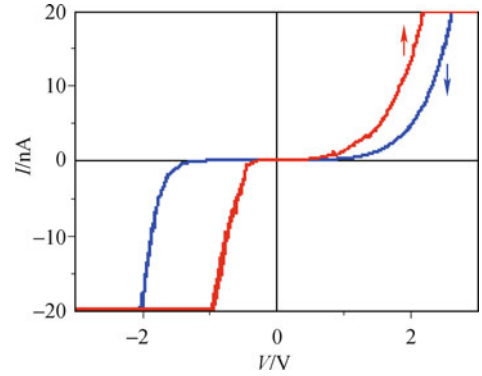

Fig. 3 I–V characteristics measured by CAFM on a $Ba_{0.95}Sr_{0.05}TiO_3/La_{0.7}Sr_{0.3}MnO_3$ sample. Arrows indicate the orientation of ferroelectricity.

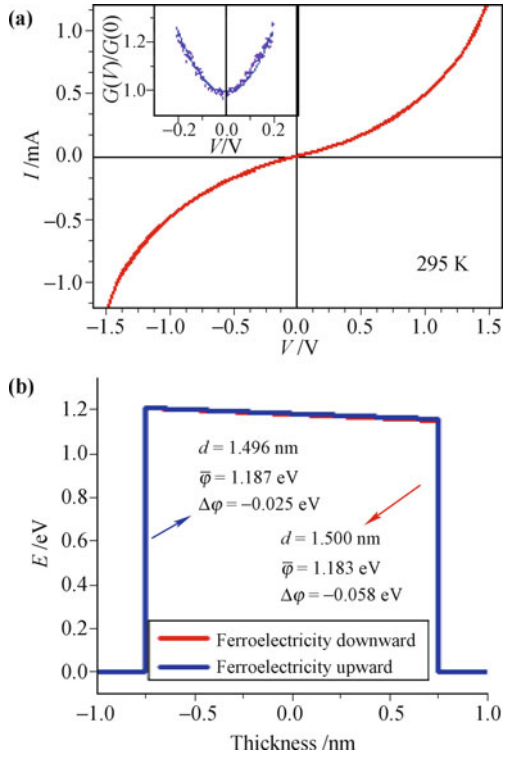

Fig. 4 **(a)** I–V curve of a $La_{0.7}Sr_{0.3}MnO_3/Ba_{0.95}Sr_{0.05}TiO_3/La_{0.7}Sr_{0.3}MnO_3$ MFTJ. Inset: Bias dependence of the normalized dynamics conductance calculated from the I–V curve (*round dots*) and fitting results by Brinkman model (*solid line*). **(b)** The barrier potential diagrams of the MFTJ with ferroelectric polarization upward and downward.

complex band structure in $Ba_{0.95}Sr_{0.05}TiO_3$. Moreover, although ± 1.4 V was used as poling voltages, we do not have direct evidence that the voltage is enough to completely poling the ferroelectric layer. Therefore, other switching mechanisms like the interfacial electrochemical modification by electric field may also take responsibility for the results [38–40]. More work is being carried on to understand the underlying mechanism.

Figure 5 shows that, by reversing the barrier polarization repeatedly, the junction resistances measured at 10 μA bias between the two polarization states can be switched between each other directly. Here, the red and blue dots means that the switching was observed between parallel and antiparallel magnetic states [reached by R–H sweep (see Fig. 6)], respectively. Hence, after applying positive and negative voltages, two parallel and two antiparallel states *i.e.* a distinct four-state device was represented.

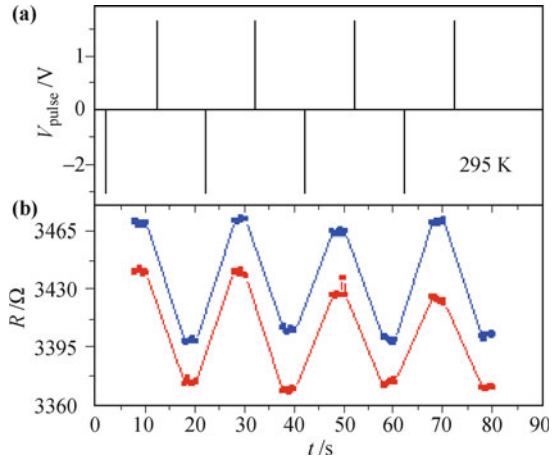

Fig. 5 In response to **(a)** the applied voltage pulses, **(b)** switching of the junction resistance (measured at 10 μA) for a $La_{0.7}Sr_{0.3}MnO_3/Ba_{0.95}Sr_{0.05}TiO_3/La_{0.7}Sr_{0.3}MnO_3$ MFTJ at parallel (*red*) and antiparallel (*blue*) states.

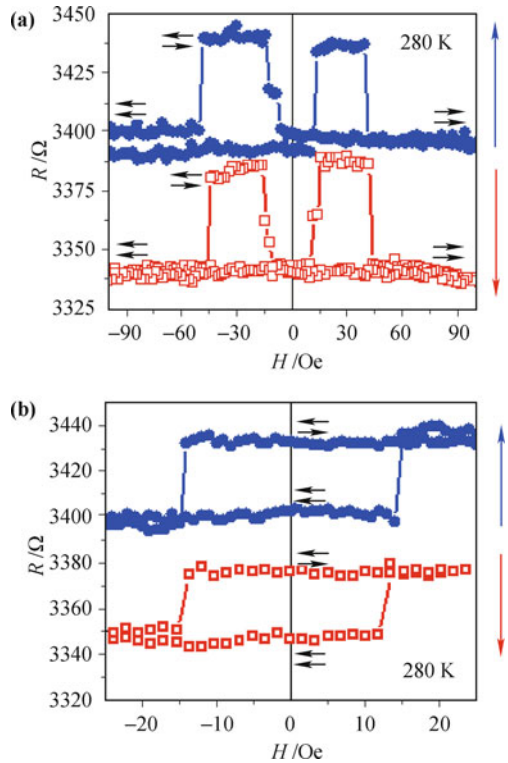

Fig. 6 R vs. H of the $La_{0.7}Sr_{0.3}MnO_3/Ba_{0.95}Sr_{0.05}TiO_3/La_{0.7}Sr_{0.3}MnO_3$ MFTJ measured at 10 mV and 280 K after poling the ferroelectricity upward (*red*) and downward (*blue*). The horizontal arrows indicate the directions of the electrode magnetization and the vertical arrows indicate the directions of the barrier polarization.

Figure 6(a) shows the magnetic field (H) dependence of the junction resistance (R) at a fixed voltage bias

of 10 mV after aligning the ferroelectric polarization of $Ba_{0.95}Sr_{0.05}TiO_3$ barrier downward or upward. A sharp resistance change against the magnetic field is observed between two magnetic states (parallel and antiparallel), suggesting an almost entire flip of the magnetic domains. After reversing the polarization of barrier, the entire R–H curve shifts so that both parallel and antiparallel resistances switched to different values and four resistance states were observed. Figure 6(b) shows two resistance memory loops (measured at 10 mV) as a function of magnetic field for the two polarization states. A standard MTJ memory loop with two states (parallel and antiparallel) is obtained for both polarization states and it can be switched between two states by sweeping magnetic field. Similar to the R–H loops in Fig. 6(a), the resistance can be switched from one memory loop to aother by reversing the ferroelectricity of the barrier. It is worth mentioning that, from Fig. 6(b), the four states can be observed at zero magnetic and electric field, which means that the memory device is non-volatile.

Larger TER and TMR effect (up to ∼300%) can be obtained at lower temperatures in the trilayer junctions [33]. Figure 7 shows the R–V_p loops of a $La_{0.7}Ca_{0.3}MnO_3/Ba_{0.5}Sr_{0.5}TiO_3/La_{0.7}Ca_{0.3}MnO_3$ MFTJ (∼ 8 μm × 8 μm in area) in parallel magnetization state at 4.2 K. Here, each data point in the hysteresis loop is tested at a fixed voltage bias [−0.1 V for Fig. 7(a), −0.15 V for Fig. 7(b)] after pulsing a voltage. The TER values decreases from 45 % to 22 % with the increasing bias from −0.1 V to −0.15 V, and are all higher than the TER at room temperature shown in Figs. 5 and 6 (∼2%) which are tested at even lower bias. The junction resistance changes when the polarization was switched by external voltage pulses and saturates afterward, indicating the coercive field for the polarization reversal should be reached. The switching voltage is slightly asymmetric, possibly due to the imprint of the ferroelectric layer.

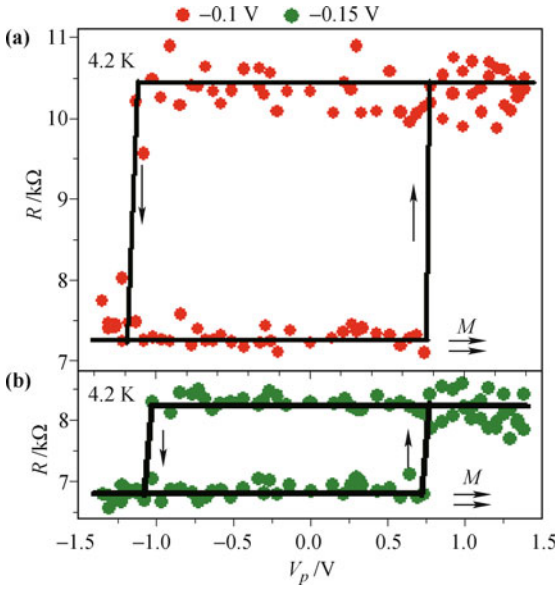

Fig. 7 R vs. V_p of a $La_{0.7}Ca_{0.3}MnO_3/Ba_{0.5}Sr_{0.5}TiO_3/La_{0.7}Ca_{0.3}MnO_3$ MFTJ at 4.2 K measured with **(a)** −0.1 V and **(b)** −0.15 V bias. The horizontal arrows indicate the directions of the electrode magnetization and the vertical arrows indicate the direction of the voltage pulse sequence. Lines are guide to the eyes.

4 Conclusions

In conclusion, we have fabricated all-oxide multiferroic tunnel junctions by pulsed laser deposition technique. Four distinct resistance states with large resistance differentials have been obtained and the device can operate at room temperatures. Using scanning probe technique, much larger TER effect can be obtained than that of the large size planner trilayer tunnel junctions. Further study on the origins of the differences should be conducted so that larger TER effect can also be obtained in trilayer junctions, which can be used in practical devices. These results pave the way for new multilevel and nonvolatile devices.

Acknowledgements The work was supported in part by DOE DE-FG02-08ER4653 (QL), NSF DMR-1207474 (QL), Penn State MRSEC seed grant (QL), and NBRP-2012CB922003 (XL), and NSFC-50831006 (ZZ).

References

1. R. Ramesh and N. A. Spaldin, Nat. Mater., 2007, 6(1): 21
2. J. A. Hutchby, R. Cavin, V. Zhirnov, J. E. Brewer, and G. Bourianoff, Computer, 2008, 41(5): 28
3. J. Ma, J. M. Hu, Z. Li, and C. W. Nan, Adv. Mater., 2011, 23(9): 1062
4. J. P. Velev, S. S. Jaswal, and E. Y. Tsymbal, Philos. Trans. R. Soc. A, 2011, 369: 3069
5. J. S. Moodera, L. R. Kinder, T. M. Wong, and R. Meservey, Phys. Rev. Lett., 1995, 74(16): 3273
6. L. Esaki, R. B. Laibowitz, and P. J. Stiles, IBM Technical Disclosure Bulletin, 1971, 13: 2161
7. D. A. Tenne, A. Bruchhausen, N. D. Lanzillotti-Kimura, A. Fainstein, R. S. Katiyar, A. Cantarero, A. Soukiassian, V. Vaithyanathan, J. H. Haeni, W. Tian, D. G. Schlom, K. J. Choi, D. M. Kim, C. B. Eom, H. P. Sun, X. Q. Pan, Y. L. Li, L. Q. Chen, Q. X. Jia, S. M. Nakhmanson, K. M. Rabe, and X. X. Xi, Science, 2006, 313(5793): 1614
8. D. D. Fong, G. B. Stephenson, S. K. Streiffer, J. A. Eastman, O. Auciello, P. H. Fuoss, and C. Thompson, Science, 2004, 304(5677): 1650
9. C. Lichtensteiger, J.M. Triscone, J. Junquera, and P. Ghosez, Phys. Rev. Lett., 2005, 94(4): 047603
10. E. Y. Tsymbal and H. Kohlstedt, Science, 2006, 313(5784): 181
11. M. Y. Zhuravlev, R. F. Sabirianov, S. S. Jaswal, and E. Y. Tsymbal, Phys. Rev. Lett., 2005, 94(24): 246802

12. J. P. Velev, C. G. Duan, K. D. Belashchenko, S. S. Jaswal, and E. Y. Tsymbal, Phys. Rev. Lett., 2007, 98(13): 137201
13. H. Kohlstedt, N. A. Pertsev, J. R. Contreras, and R. Waser, Phys. Rev. B, 2005, 72(12): 125341
14. V. Garcia, S. Fusil, K. Bouzehouane, S. Enouz-Vedrenne, N. D. Mathur, A. Barthélémy, and M. Bibes, Nature, 2009, 460(7251): 81
15. A. Gruverman, D. Wu, H. Lu, Y. Wang, H. W. Jang, C. M. Folkman, M. Y. Zhuravlev, D. Felker, M. Rzchowski, C. B. Eom, and E. Y. Tsymbal, Nano Lett., 2009, 9(10): 3539
16. A. Chanthbouala, A. Crassous, V. Garcia, K. Bouzehouane, S. Fusil, X. Moya, J. Allibe, B. Dlubak, J. Grollier, S. Xavier, C. Deranlot, A. Moshar, R. Proksch, N. D. Mathur, M. Bibes, and A. Barthelemy, Nat. Nanotechnol., 2012, 7(2): 101
17. P. Maksymovych, S. Jesse, P. Yu, R. Ramesh, A. P. Baddorf, and S. V. Kalinin, Science, 2009, 324(5933): 1421
18. A. Crassous, V. Garcia, K. Bouzehouane, S. Fusil, A. H. G. Vlooswijk, G. Rispens, B. Noheda, M. Bibes, and A. Barthelemy, Appl. Phys. Lett., 2010, 96(4): 042901
19. J. P. Velev, C. G. Duan, J. D. Burton, A. Smogunov, M. K. Niranjan, E. Tosatti, S. S. Jaswal, and E. Y. Tsymbal, Nano Lett., 2009, 9(1): 427
20. H. Zheng, J. Wang, S. E. Lofland, Z. Ma, L. Mohaddes-Ardabili, T. Zhao, L. Salamanca-Riba, S. R. Shinde, S. B. Ogale, F. Bai, D. Viehland, Y. Jia, D. G. Schlom, M. Wuttig, A. Roytburd, and R. Ramesh, Science, 2004, 303(5658): 661
21. C. G. Duan, S. S. Jaswal, and E. Y. Tsymbal, Phys. Rev. Lett., 2006, 97(4): 047201
22. J. M. Rondinelli, M. Stengel, and N. A. Spaldin, Nat. Nanotechnol., 2008, 3(1): 46
23. C. A. F. Vaz, J. Hoffman, C. H. Anh, and R. Ramesh, Adv. Mater., 2010, 22(26–27): 2900
24. C. W. Nan, M. I. Bichurin, S. X. Dong, D. Viehland, and G. Srinivasan, J. Appl. Phys., 2008, 103(3): 031101
25. K. F. Wang, J. M. Liu, and Z. F. Ren, Adv. Phys., 2009, 58(4): 321
26. M. Bibes, J. E. Villegas, and A. Barthelemy, Adv. Phys., 2011, 60(1): 5
27. M. Gajek, M. Bibes, S. Fusil, K. Bouzehouane, J. Fontcuberta, A. E. Barthélémy, and A. Fert, Nat. Mater., 2007, 6(4): 296
28. V. Garcia, M. Bibes, L. Bocher, S. Valencia, F. Kronast, A. Crassous, X. Moya, S. Enouz-Vedrenne, A. Gloter, D. Imhoff, C. Deranlot, N. D. Mathur, S. Fusil, K. Bouzehouane, and A. Barthélémy, Science, 2010, 327(5969): 1106
29. S. Valencia, A. Crassous, L. Bocher, V. Garcia, X. Moya, R. O. Cherifi, C. Deranlot, K. Bouzehouane, S. Fusil, A. Zobelli, A. Gloter, N. D. Mathur, A. Gaupp, R. Abrudan, F. Radu, A. Barthélémy, and M. Bibes, Nat. Mater., 2011, 10(10): 753
30. D. Pantel, S. Goetze, D. Hesse, and M. Alexe, Nat. Mater., 2012, 11(4): 289
31. M. Hambe, A. Petraru, N. A. Pertsev, P. Munroe, V. Nagarajan, and H. Kohlstedt, Adv. Funct. Mater., 2010, 20(15): 2436
32. J. H. Park, E. Vescovo, H. J. Kim, C. Kwon, R. Ramesh, and T. Venkatesan, Nature, 1998, 392(6678): 794
33. W. J. Hu, K. Chen, Z. D. Zhang, X. X. Xi, and Q. Li, unpublished
34. Y. W. Yin, M. Raju, W. J. Hu, X. J. Weng, X. G. Li, and Q. Li, J. Appl. Phys., 2011, 109: 07D915
35. E. T. Wertz, and Q. Li, Appl. Phys. Lett., 2007, 90(14): 142506
36. M. Y. Zhuravlev, Y. Wang, S. Maekawa, and E. Y. Tsymbal, Appl. Phys. Lett., 2009, 95(5): 052902
37. W. F. Brinkman, R. C. Dynes, and J. M. Rowell, J. Appl. Phys., 1970, 41(5): 1915
38. J. Z. Sun, K. P. Roche, and S. S. P. Parkin, Phys. Rev. B, 2000, 61(17): 11244
39. H. Kohlstedt, A. Petraru, K. Szot, A. Rudiger, P. Meuffels, H. Haselier, R. Waser, and V. Nagarajan, Appl. Phys. Lett., 2008, 92(6): 062907
40. J. Choi, J. S. Kim, I. Hwang, S. Hong, I. S. Byun, S. W. Lee, S. O. Kang, and B. H. Park, Appl. Phys. Lett., 2010, 96(26): 262113